Proceedings of HT2005
2005 ASME Summer Heat Transfer Conference
July 17-22, 2005, San Francisco, California, USA

HT2005-72395

Three-Dimensional Modeling of Laser Sintering of a Two-Component Metal Powder Layer on Top of Sintered Layers

Tiebing Chen and Yuwen Zhang
Department of Mechanical and Aerospace Engineering
University of Missouri-Columbia
Columbia, MO 65211
Email: zhangyu@missouri.edu

ABSTRACT

A three-dimensional numerical model of Selective Laser Sintering (SLS) of the metal powders for a single scan line induced by a moving laser beam interacted with a loose powder layer on top of the sintered metal layers is presented. The problem is modeled using a temperature-transforming model and the partial shrinkage induced by melting is accounted for. The heat losses at the top surface due to the natural convection and radiation are taken into account. The liquid flow of the molten low melting point metal powders, which is driven by capillary and gravity forces, is also considered and formulated by using Darcy's law. The effects of the dominant processing parameters, such as the moving heat source intensity, scanning velocity and number of the existing sintered layers underneath are investigated. A parametric study is performed and the best combination of the processing parameters is recommended.

INTRODUCTION

Selective Laser Sintering (SLS) is a layered manufacturing method that creates solid, three-dimensional objects by fusing powdered materials with a moving laser (CO_2 or YAG) beam [1]. During the SLS process, a thin (100 - 250 μm thick) powder layer is laser-scanned to fuse the two-dimensional slice to an underlying solid piece, which consists of a series of stacked and fused two-dimensional slices. After laser scanning, a fresh powder layer is spread and the scanning process is repeated. Loose powder is removed after the part is extracted from its bin. A brief review of the basic principles of SLS machine operation, and materials issues affecting direct SLS of metals and the resultant properties and microstructures of the parts are discussed by Agarwala *et al.* [2]. An overview of the latest progress on selective laser sintering (SLS) work as reported in various journals and proceedings is presented by Kumar [3].

Melting and resolidification are the mechanisms to bond metal powder particles to form a layer of part and also the mechanisms to bond different layers together to form a functional part. Fundamentals of melting and solidification have been investigated extensively and detailed reviews are available in the literatures [4, 5]. The distinctive feature of laser-induced melting of the metal powders is that it is always accompanied with the shrinkage due to the significant density change. When a single-component metal powder system is used the SLS process, what is left behind after laser scanning is a series of spheres with diameter comparable to the size of the laser beam and this is referred to as balling phenomenon [6]. In order to avoid this balling phenomenon, the powder mixture which is composed of two types of powders that possess significantly different melting points was suggested by Bunnell [7] and Manzur *et al.* [8]. In case of two-component sintering, a molten liquid is formed by fully melting the powders possessing the lower melting point, which infiltrates into the voids between the solid powders with higher melting point and binds them together. Meanwhile, the solid particles will move downward because of the shrinkage due to the significant density change. It should be noted that only the low-melting-point powder melts and resolidifies in SLS and the high melting point powder is solid throughout the process. A one-dimensional thermal model of melting of the two-component powder bed was presented by Pak and Plumb [9], in which the liquid motion driving by capillary and gravity forces is considered but the shrinkage was neglected. Zhang and Faghri analytically solved the one-dimensional melting of a semi-infinite two-component metal powder bed heated by the constant heat flux [10]. Chen and Zhang [11] obtained the analytical solution of one-dimensional melting of the two-component metal powder bed with finite thickness subjected to constant heat flux. Zhang and Faghri [12] simulated two-

dimensional melting and resolidification of a subcooled two-component metal powder bed with a moving Gaussian heat source with shrinkage accounted for but the liquid flow of the low melting point metal is neglected. A three-dimensional finite element simulation for temperature evolution in the SLS process was demonstrated by Kolossov *et al.* [13], who considered the non-linear behavior of thermal conductivity and of specific heat due to temperature changes and phase transformations. A three-dimensional thermal model of SLS of two-component metal powder bed was presented by Zhang *et al.* [14], who considered the effects of the solid particle velocity induced by shrinkage of the powder bed and a liquid flow driven by capillary and gravity forces on the SLS process.

The thickness of the powder bed used in Ref. [14] was very large, which approximated the sintering process of the first layer with the complete shrinkage. In reality, SLS is a layer-by-layer process by which the sintering process occurs in a fresh loose powder layer on top of multiple sintered layers. Numerical solution of a three-dimensional quasi-steady state melting and resolidification problem in a two-component metal powder layer on the top of multiple sintered layers subjected to a moving Gaussian laser beam will be presented in this paper. The effects of the volume fraction of the gas in the Heat Affected Zone (HAZ), laser scanning velocity and the number of the existing sintered layers on the shape of the Heat Affected Zone (HAZ) will be investigated.

NOMENCLATURE

Bi	Biot number, hR/k_H
Bo	Bond Number, $\rho_\ell g R d_p/\gamma_m^0$
C	dimensionless heat capacity, C^0/C_H^0
C^0	heat capacity, ρc_p, $(J/m^3\text{-}K)$
c_p	specific heat, $(J/kg\text{-}K)$
d_p	diameter of the powder particle (m)
g	gravitational acceleration (m/s^2)
h	convective heat transfer coefficient, $(W/m^2\text{-}K)$
$h_{s\ell}$	latent heat of melting or solidification, J/kg
i	unit vector in x direction
I_0	laser intensity at the center of the laser beam, (W/m^2)
j	unit vector in y direction
k	thermal conductivity, (W/mK)
k	unit vector in z direction
K	permeability, or dimensionless thermal conductivity, k/k_H
$K_{r\ell}$	relative permeability
Ma	Marangoni number, $\gamma_m^0 d_p/(\alpha_H \mu)$
N	number of existing sintered layers
N_i	dimensionless laser intensity, $\alpha_a I_0 R/[k_H(T_m^0-T_i^0)]$
N_R	radiation number, $\varepsilon_e\sigma(T_m^0-T_i^0)^3 R/k_H$
N_t	temperature ratio for radiation, $T_m^0/(T_m^0-T_i^0)$
p	pressure (N/m^2)
P_c	dimensionless capillary pressure, $p_c/(\gamma_m^0\sqrt{\varepsilon/K})$
R	radius of the moving laser beam at 1/e (m)
s	solid-liquid interface location (m)
s_0	location of surface (m)
s_{st}	sintered depth (m)
S	Source term
Sc	subcooling parameter, $C_L^0(T_m^0-T_i^0)/(\rho_L h_{s\ell})$
T	dimensionless temperature, $(T^0-T_m^0)/(T_m^0-T_i^0)$
t	false time (s)
T^0	temperature (K)
u_b	laser beam moving velocity (m/s)
U_b	dimensionless heat source moving velocity, $u_b R/\alpha_H$
$\mathbf{v}$	velocity vector, $u\mathbf{i}+v\mathbf{j}+w\mathbf{k}$
$\mathbf{V}$	dimensionless velocity vector, $\mathbf{v}R/\alpha_H$
$\forall$	volume (m^3)
W	shrinkage velocity
x, y, z	coordinate, (m)
X, Y, Z	dimensionless moving horizontal coordinate, $(x, y, z)/R$

Greek symbol

α	thermal diffusivity $(m^2\,s^{-1})$
α_a	absorbtivity
γ^0	surface tension, (N/m^2)
γ	dimensionless surface tension, γ^0/γ_m^0
γ_m^0	surface tension of the low melting point metal at melting point, (N/m^2)
δ	powder layer thickness, (m)
Δ	dimensionless powder layer thickness, δ/R
ΔT^0	one-half of phase-change temperature range (K)
ΔT	one-half of dimensionless phase change temperature range
ε	porosity for unsintered powder, $(\forall_g+\forall_\ell)/(\forall_g+\forall_\ell+\forall_s+\forall_H)$
ε_e	emissivity of surface
η	dimensionless location of the solid-liquid interface, s/R
η_0	dimensionless location of the surface, s_0/R
η_{st}	dimensionless sintered depth, s_{st}/R
ρ	density (kg/m^3)
σ	Stefan-Boltzmann constant, $5.67\times10^{-8}\,W/(m^2\text{-}K^4)$

τ dimensionless false time, $\alpha_H t / R^2$

φ volume fraction

$\dot{\Phi}_L$ dimensionless volume production rate of the liquid

ψ saturation, φ_l / ε

∇ dimensionless gradient operator, $\mathbf{i}(\partial/\partial X)+\mathbf{j}(\partial/\partial Y)+\mathbf{k}(\partial/\partial Z)$

Subscripts

c capillary

g gas(es)

eff effective

H high melting point powder

i initial

ℓ liquid or sintered region

L low melting point powder

m melting point

p existing sintered region

s solid

PHYSICAL MODEL

Figure 1 shows the physical model of the laser sintering problem under consideration. The sintering process is modeled in a single loose powder layer with multiple previously sintered layers underneath. A moving circular Gaussian laser beam with the scanning velocity, u_b, is considered and a moving coordinate system is adopted. The partial shrinkage is considered in the physical model, i.e., the fraction of the gas trapped in the heat affected zone (HAZ) is different. The porosity in the liquid pool, which is defined as volume fraction of gas and low melting point liquid, is no longer the same as that of the loose powder all the time as was the case in Ref. [14]. A single line scanning of the laser beam is considered, therefore, half of the physical domain is considered because of the symmetry.

The temperature transforming model is used to formulate the physical model [15]. The dimensionless governing equation in the moving coordinate system can be described as

$$\nabla\cdot(\varphi_\ell \mathbf{V}_\ell C_L T)-U_b\frac{\partial}{\partial X}[(\varphi_H+\varphi_s C_L)T]+W_s\frac{\partial}{\partial Z}[(\varphi_H+\varphi_s C_L)T]$$
$$=\nabla\cdot(K\nabla T)-\left\{\frac{\partial}{\partial\tau}[(\varphi_\ell+\varphi_s)S]+\nabla\cdot(\varphi_\ell\mathbf{V}_\ell S)+W_s\frac{\partial}{\partial Z}(\varphi_s S)-U\frac{\partial}{\partial X}[(\varphi_\ell+\varphi_s)S\right\} \quad (1)$$

where the dimensionless variables are defined in the nomenclature. The dimensionless shrinkage velocity, W, heat capacity, C, source term, S, and thermal conductivity, K, in eq. (1) in the loose powder layer are different from those in existing sintered layers below, which have been fully solidified. In the loose powder layer,

$$W_s=\begin{cases}0, & Z>S\\ \dfrac{1-\varepsilon_\ell-\varphi_{H,i}}{1-\varepsilon_\ell}\left(\dfrac{\partial S}{\partial\tau}-U_b\dfrac{\partial S}{\partial X}\right), & Z<S\end{cases} \quad (2)$$

$$C_L=\begin{cases}C_L & T<-\Delta T\\ C_L\left(1+\dfrac{1}{2\,Sc\,\Delta T}\right) & -\Delta T<T<\Delta T\\ C_L & T>\Delta T\end{cases} \quad (3)$$

$$S=\begin{cases}0 & T<-\Delta T\\ \dfrac{C_L}{2\,Sc} & -\Delta T<T<\Delta T\\ \dfrac{C_L}{Sc} & T>\Delta T\end{cases} \quad (4)$$

$$K=\begin{cases}K_{eff} & T<-\Delta T\\ K_{eff}+\dfrac{K_\ell-K_{eff}}{2\Delta T}(T+\Delta T) & -\Delta T<T<\Delta T\\ K_\ell & T>\Delta T\end{cases} \quad (5)$$

$$K_\ell=(\varphi_\ell+\varphi_s)K_L+\varphi_H \quad (6)$$

where k_{eff} can be referred to Ref. [16].

In the resolidified region at the left side of liquid pool and underneath the loose powder layer,

$$W=0 \quad (7)$$

$$C=C_L \quad (8)$$

$$S=\frac{C_L}{Sc} \quad (9)$$

$$K=K_\ell \quad (10)$$

The dimensionless velocities of the liquid phase, $\mathbf{V}_\ell$, can be obtained by Darcy's law. The dimensionless equation of Darcy's law is

$$\mathbf{V}_\ell-(-U_b\mathbf{i}+W_s\mathbf{k})=\frac{\varepsilon\,Ma\,\psi_e^3}{\sqrt{180}(1-\varepsilon)^2\psi}\nabla P_c+\frac{\varepsilon^2\,Ma\,Bo\,\psi_e^3}{180(1-\varepsilon)^2\psi}\mathbf{k} \quad (11)$$

where

$$Ma=\frac{\gamma_m^0\,d_p}{\alpha_H\mu},\quad Bo=\frac{\rho_\ell g\,R\,d_p}{\gamma_m^0} \quad (12)$$

are Marangoni and Bond numbers, respectively.

The dimensionless capillary pressure, P_c, in eq. (11) can be calculated by [17],

$$P_c=\frac{\gamma_m^0}{(K/\varepsilon)^{1/2}}\left[1.417(1-\psi_e)-2.12(1-\psi_e)^2+1.263(1-\psi_e)^3\right] \quad (13)$$

where the normalized saturation, ψ_e, in eq. (11) is obtained by

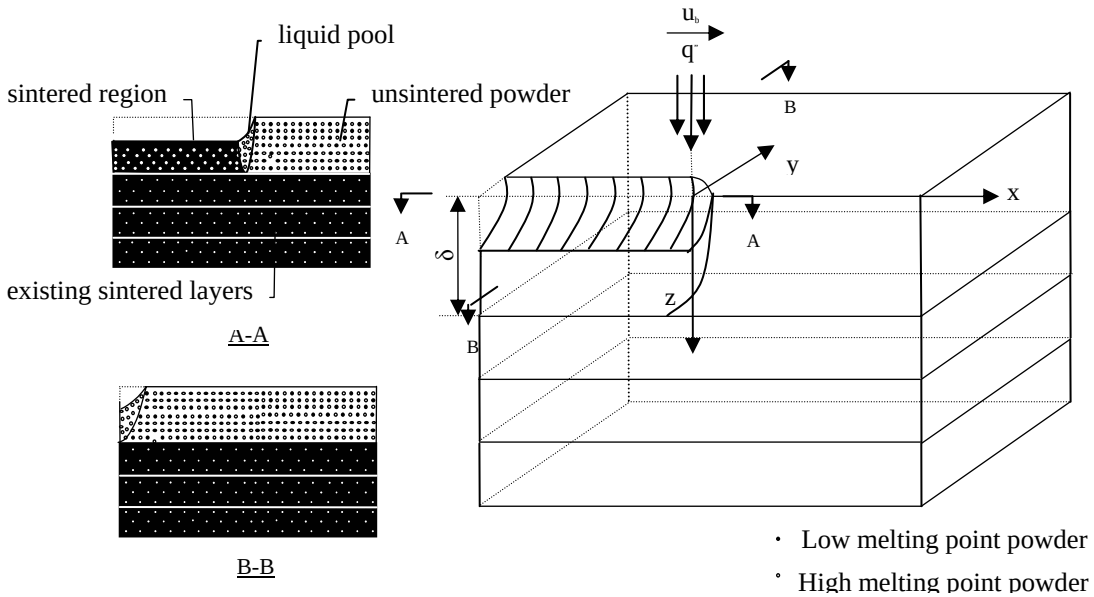

Fig.1 Physical Model

$$\psi_e = \begin{cases} \dfrac{\psi - \psi_{ir}}{1-\psi_{ir}} & \psi > \psi_{ir} \\ 0 & \psi \le \psi_{ir} \end{cases} \tag{14}$$

Equation (11) satisfies the dimensionless continuity equation of the liquid in the moving coordinate system, which is obtained by

$$\frac{\partial \varphi_\ell}{\partial \tau} - U_b \frac{\partial \varphi_\ell}{\partial X} + \nabla \cdot (\varphi_\ell \mathbf{V}_\ell) = \dot{\Phi}_L \tag{15}$$

The continuity equations for the solid phase of the low melting point powder and high melting point powder by assuming shrinkage occurs in the z- direction only are

$$\frac{\partial \varphi_s}{\partial \tau} - U_b \frac{\partial \varphi_s}{\partial X} + \frac{\partial (\varphi_s w_s)}{\partial Z} = -\dot{\Phi}_L \tag{16}$$

$$\frac{\partial \varphi_H}{\partial \tau} - U_b \frac{\partial \varphi_H}{\partial X} + \frac{\partial (\varphi_H w_s)}{\partial Z} = 0 \tag{17}$$

and the following relationship is valid in all regions

$$\varepsilon + \varphi_s + \varphi_H = 1 \tag{18}$$

Combined with eqs.(6-8), the volume production rate, $\dot{\Phi}_L$, is obtained:

$$\dot{\Phi}_L = -\frac{\partial (1-\varepsilon)}{\partial \tau} + U_b \frac{\partial (1-\varepsilon)}{\partial X} - \frac{\partial}{\partial Z}\left[(1-\varepsilon) W_s\right] \tag{19}$$

where the porosity, ε, is not constant during the sintering process under the partial shrinkage model. Since the porosity, ε, is defined as volume fraction of void that can be occupied by either gas or liquid, the value of the porosity depends upon the volume fraction of the gas in the loose powders or HAZ. The porosity in the loose powder layer, ε_s is equal to the initial volume fraction of the gas in the powders, $\varphi_{g,s}$. The porosity in HAZ can be calculated from $\varepsilon_\ell = \varphi_\ell + \varphi_{g,\ell}$.

The corresponding boundary and initial conditions of eq. (1) are

$$-K\frac{\partial T}{\partial Z} = N_i \exp(-X^2) - N_R[(T+N_t)^4 - (T_\infty + N_t)^4] - Bi(T - T_\infty) \quad Z = \eta_0(X) \tag{20}$$

$$\frac{\partial T}{\partial Z} = 0 \ , -\infty < X < \infty, \ 0 \le Y < \infty, \ Z = \Delta_s + N\Delta_\ell, \ \tau > 0 \tag{21}$$

$$T = -1, -\infty < X < \infty, 0 \le Y < \infty, Z = \Delta_s + N\Delta_\ell, \tau = 0 \tag{22}$$

The location of liquid surface is related to the sintered depth with the assumption that the sintered layers are fully solidified, i.e.,

$$\eta_0(X,Y) = \begin{cases} \dfrac{1-\varepsilon_\ell - \varphi_{H,i}}{1-\varepsilon_\ell}\eta_{st}(X,Y) & \eta_{st} < \Delta_s \\ \dfrac{1-\varepsilon_\ell - \varphi_{H,i}}{1-\varepsilon_\ell}\Delta_s & \eta_{st} \ge \Delta_s \end{cases} \tag{23}$$

NUMERICAL SOLUTION

The fabrication of functional part is relying on a layer-by-layer SLS process. The newly sintered layer should integrate tightly with the previously deposited layers underneath for strong mechanical properties. The anticipated processing parameters, i.e., laser power intensity and scanning velocity, should ensure to obtain the ideal sintering depth which is

beyond the bottom surface of the loose powder layer. In order to obtain the expected sintering depth, the optimum combination of dimensionless laser beam intensity and scanning velocity is required. The governing equation with the false transient term in the moving coordinate system is solved by the finite volume method and the converged steady-state solution is declared when the temperature distribution doesn't change with the false transient time. With each pair of prescribed processing parameters, i.e., laser power intensity and scanning velocity, the solution is assumed to be at the steady state when the relative error of the difference between the current sintering depth with the one which is at 30 time steps before is less than 0.001. The false transient time step in the paper is 0.12. Therefore, the dimensionless laser power intensity is increased in small increments in order to obtain the expected sintering depth when the sintering depth dose not move down. The computation can be stopped when 50% overlap between HAZ and existing sintered layers underneath. The different regions, i.e., liquid pool, re-solidified region and unsintered powders, are tracked by monitoring temperature, T, which is compared with ΔT. Since the physical domain is irregular shape due to the movement of the top surface, a block-off technique [18] is used to simply the computation. The thermal conductivity in the empty space created by the shrinkage is zero.

RESULTS AND DISCUSSIONS

The effects of the volume fraction of the gas in the liquid combined with the scanning velocity of the moving laser beam and the number of the existing sintered layers underneath on the formation of the Heat Affected Zone (HAZ) are investigated. The powders, i.e., Nickel Braze and AISI 1018, are applied in the present paper. The Nickel Braze is the low melting point powder and AISI 1018 is the high melting point powder. The thermal properties of the Nickel Braze and AISI 1018 are available in the reference [14]. The dimensionless parameters that are used in the numerical simulation are shown in Table 1.

Table 1 Sintering parameters applied in the numerical simulation

B_i	2.94×10^{-4}	N_R	4.2×10^{-4}
Bo	5.3×10^{-3}	Sc	1.38
C_L	1.07	T_∞	-1.0
K_g	5.38×10^{-4}	φ_{gs}	0.42
K_L	0.2	$\varphi_{g,\ell}$	0.0, 0.2, 0.42
Mc	1042.0	ψ_{ir}	0.08
N_g	1.19×10^{-3}	ΔT	0.001
N	1, 3		

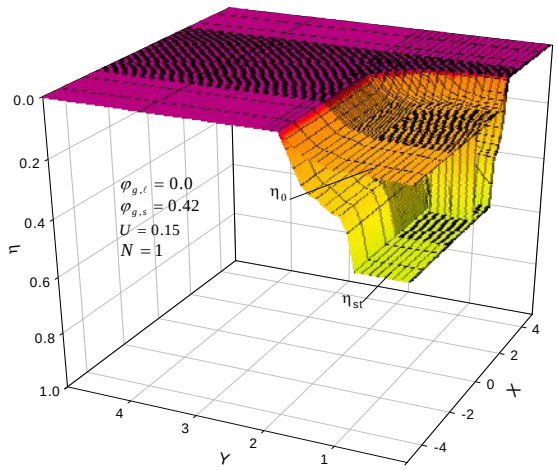

(a)

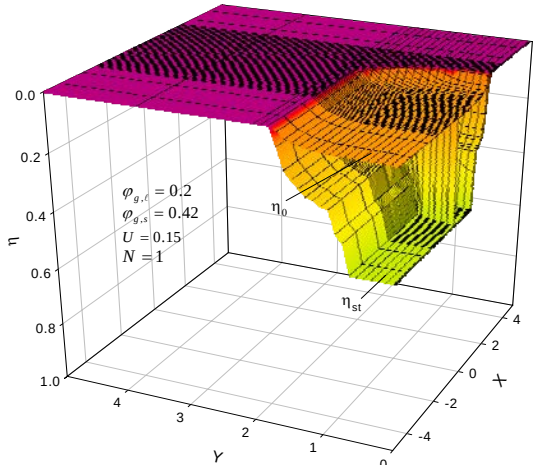

(b)

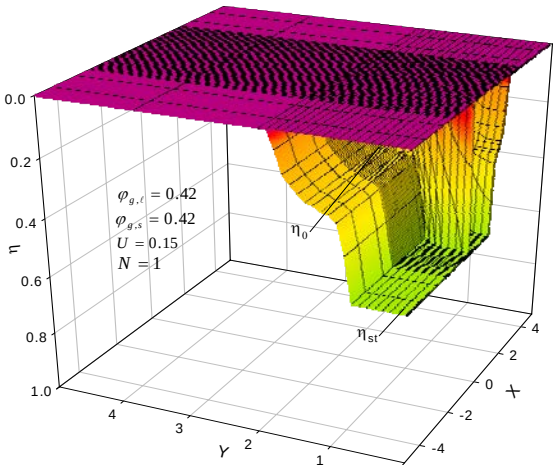

(c)

Fig. 2 Three-dimensional shape of the HAZ ($\Delta_s = 0.25$, $U = 0.1$, $N = 1$)

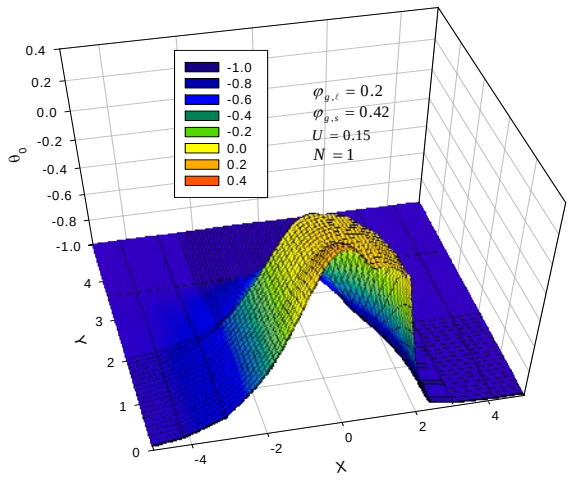

Fig. 3 The temperature distribution at the surface of the powder layer ($\Delta_s = 0.25$, $U = 0.1$, $\varphi_{g\ell} = 0.2$)

The three dimensional shape of the Heat Affected Zone (HAZ) sintered by a moving circular laser beam with respect to different volume fraction of the gas in the liquid pool with one existing sintered layer below are shown in Fig. 2. The overlap between the liquid pool and existing sintered layers below are considered in order to bond the newly deposited layer with the existing sintered layers tightly. The shrinkage is smaller when the volume fraction of gas in the liquid pool increases. There is no shrinkage when the volume fractions of gas in the liquid pool and the loose powder are equal since the gas trapped in the void among the powder particles are not released. The higher moving laser beam intensity is needed for the sintering process with higher volume fraction of the gas in the liquid pool in order to obtain the same sintering depth. That is because the higher volume fraction of the gas in the liquid pool causes the smaller rate of the shrinkage and thicker existing sintered layers below. Besides, the higher magnitude of the laser power is needed since the thermal conductivity of the existed sintered layers is much higher than that of the loose powder layer. The temperature distribution on the surface of the powder layer at the quasi-steady-state during the sintering process is shown in the Fig. 3. The temperature distributed on the top surface of the overlap region of the liquid pool is higher than that of other locations since the high thermal conductivity of the existing sintered layer causes higher temperature to induce the re-melting of the existed sintered layers.

The effect of scanning velocity on the sintering process with respect to the specific fraction of the gas in the liquid pool is illustrated by the longitudinal and sectional plots of HAZ. Figure 4 shows the effect of the dimensionless scanning velocity on the sintering process for the case with the complete shrinkage ($\varphi_{g,\ell} = 0.0, N = 1$). The higher laser beam intensity is needed when the scanning velocity increases in order to achieve the desired sintering depth and overlap. The shapes of HAZ are similar but the liquid pool is a little narrower when the scanning velocity increases. That is because the time of the interaction between the moving laser beam and the powder layer is shorter. It can be seen the overlapped region of the liquid pool has reached the bottom of the physical domain when the quasi-steady-state is achieved. The effects of the dimensionless scanning velocity on the sintering process for the case with the partial shrinkage ($\varphi_{g,\ell} = 0.2, N = 1$) and without shrinkage ($\varphi_{g,\ell} = 0.42, N = 1$) are shown in Fig. 5 and Fig. 6 respectively. It can be seen the shrinkage decreases with increasing $\varphi_{g,\ell}$. The shrinkage diminishes when $\varphi_{g,\ell} = \varphi_{g,s}$. The larger laser beam intensity is needed when $\varphi_{g,\ell}$ increases since the thickness of the existing sintered layers underneath increases. The similar phenomena happened in Fig. 4 can also be observed.

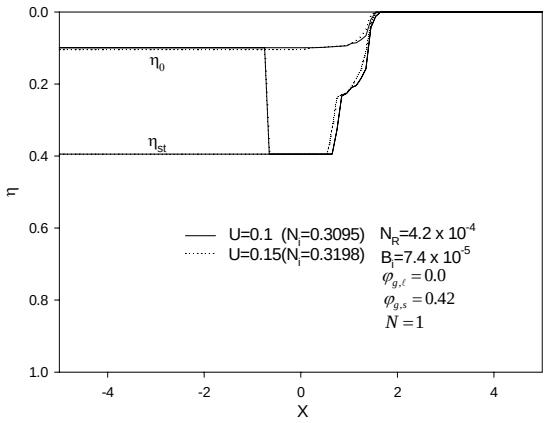

(a)

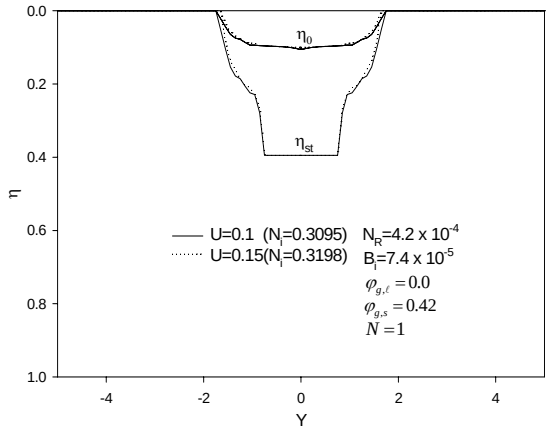

(b)

Fig. 4 Effects of laser intensity and scanning velocity on the sintering process ($\varphi_{g\ell} = 0.0$, $N = 1$)

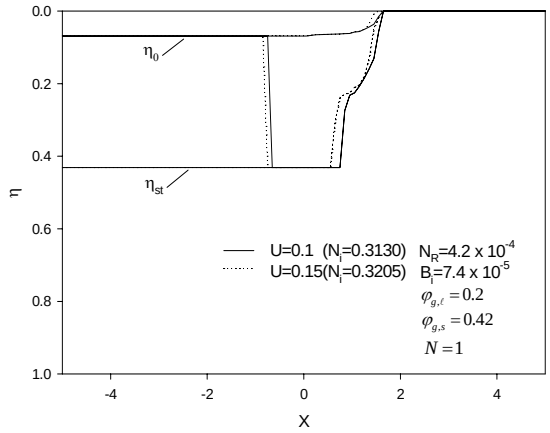

(a)

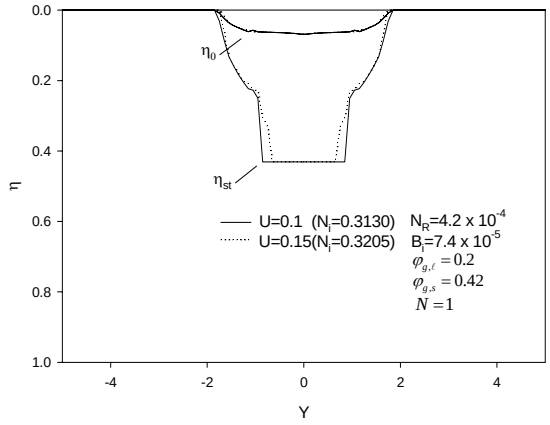

(b)

Fig. 5 Effects of laser intensity and scanning velocity on the sintering process ($\varphi_{g\ell} = 0.2,\ N = 1$)

Figure 7-9 shows the effect of the dimensionless scanning velocity on the sintering process for the cases with the complete shrinkage ($\varphi_{g,\ell} = 0.0, N = 3$), partial shrinkage ($\varphi_{g,\ell} = 0.2, N = 3$) and without the shrinkage ($\varphi_{g,\ell} = 0.42, N = 3$) when the number of the existing sintered layers increases. It can be seen that the laser beam intensity increases significantly when the number of existed sintered layers below increases. The higher scanning velocity needs the higher laser beam intensity. The liquid pool also moves slightly toward the positive direction of the X direction. For the case without the shrinkage, the bottom of the overlapped region of HAZ is not flat since the required overlap between the newly sintered layer and existing sintered layers has been achieved before it reaches the bottom surface of the physical domain. The increase number of the existing sintered layers underneath combined with increasing $\varphi_{g,\ell}$ will demand much higher laser beam intensity. Therefore, it is always necessary to increase the shrinkage in order to achieve both highly densified sintered part and lowering the laser beam intensity at the same time.

CONCLUSIONS

The three-dimensional sintering process of the two-component metal powders for a single scan line induced by a moving laser beam interacted with a loose powder layer on top of the existing sintered metal layers is presented. The partial shrinkage due to the different fraction of the gas in HAZ and the liquid metal flow driven by capillary and gravitational forces are taken into account in the physical model. The results demonstrate that the shape of HAZ significantly affected by the fraction of the gas in the liquid pool and processing parameters such as the laser beam intensity, the scanning velocity and the number of the existing layers below. The optimized combination of the laser beam intensity and the scanning velocity with the specific number of existed sintered layers below to achieve the required sintering depth is recommended.

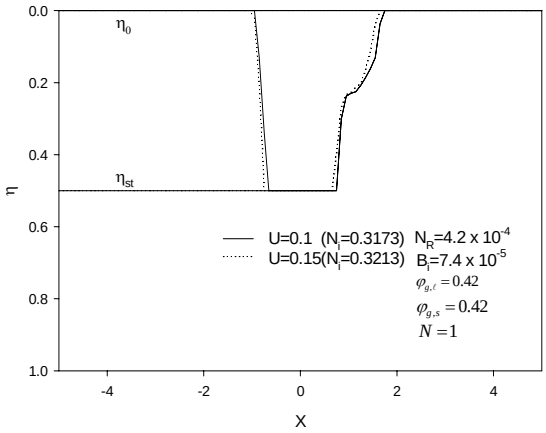

(a)

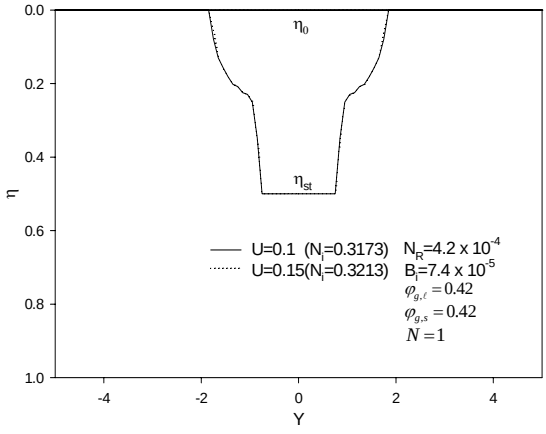

(b)

Fig. 6 Effects of laser intensity and scanning velocity on the sintering process ($\varphi_{g\ell} = 0.42,\ N = 1$)

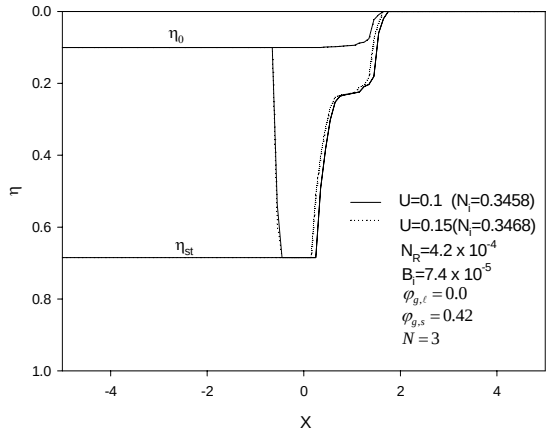

(a)

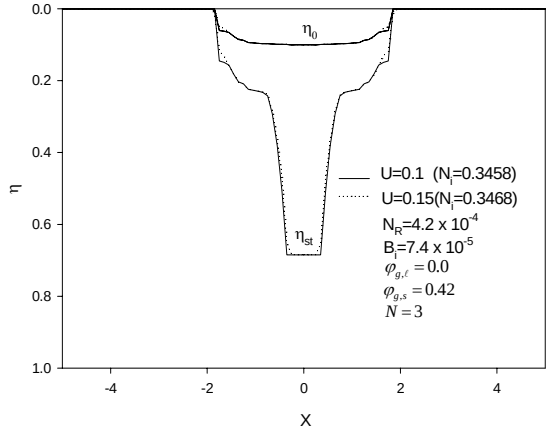

(b)

Fig. 7 Effects of laser intensity and scanning velocity on the sintering process ($\varphi_{g\ell} = 0.0$, $N = 3$)

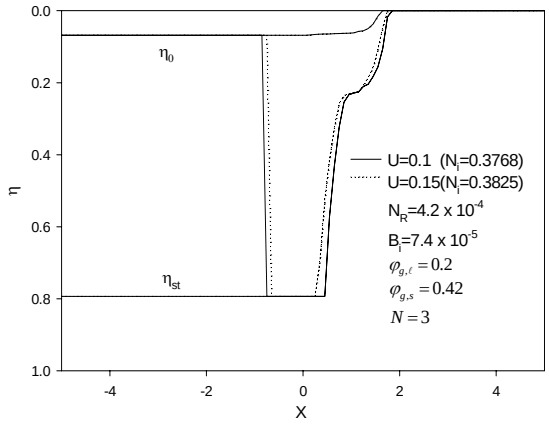

(a)

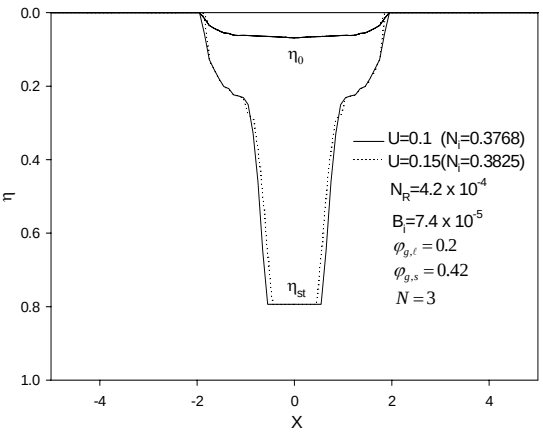

(b)

Fig.8 Effects of laser intensity and scanning velocity on the sintering process ($\varphi_{g\ell} = 0.2$, $N = 3$)

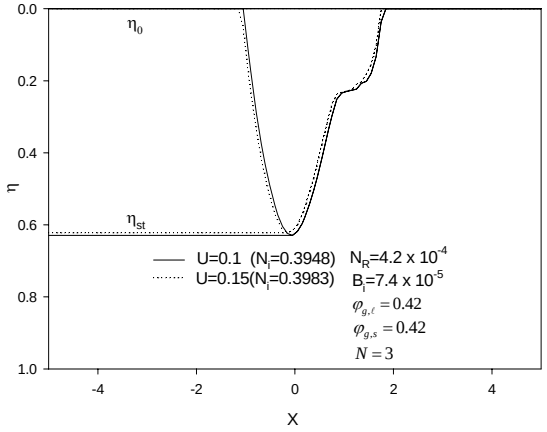

(a)

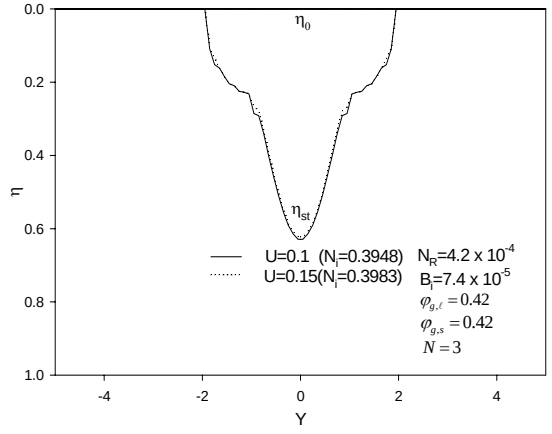

(b)

Fig.9 Effects of laser intensity and scanning velocity on the sintering process ($\varphi_{g\ell} = 0.42$, $N = 3$)

ACKNOWLEDGEMENT

Support for this work by the Office of Naval Research (ONR) under grant number N00014-04-1-0303 is gratefully acknowledged.

REFERENCES

[1] Conley, J., and Marcus, H., 1997, "Rapid Prototyping and Solid Freeform Fabrication," *Journal of Manufacturing Science and Engineering*, Vol. 119, pp. 811-816.

[2] Agarwala M., Bourell D., Beaman J., Marcus H. and Barlow J., 1995, "Direct Selective Laser Sintering of Metals," *Rapid Prototyping Journal*, Vol. 1, pp. 26-36.

[3] Kumar S., 2003, "Selective Laser Sintering: A Qualitative and Objective Approach," *JOM*, Vol. 55, pp. 43-47.

[4] Viskanta, R., 1983, Phase Change Heat Transfer, in: G.A. Lane (Ed.), *Solar Heat Storage: Latent Heat Materials*, CRC Press, Boca Raton, FL.

[5] Yao, L. C., and Prusa, J., 1989, "Melting and Freezing," *Advances in Heat Transfer*, Vol. 25**,** pp1-96.

[6] Bourell, D.L., Marcus, H.L., Barlow, J.W., and Beaman, J.J., 1992, "Selective Laser Sintering of Metals and Ceramics," *International Journal of Powder Metallurgy*, Vol. 28, No.4, pp. 369-81.

[7] Bunnell, D.E., 1995, *Fundamentals of Selective Laser Sintering of Metals*, Ph.D. Thesis, University of Texas at Austin.

[8] Manzur, T., DeMaria, T., Chen, W., and Roychoudhuri, C., 1996, "Potential Role of High Powder Laser Diode in Manufacturing," presented at SPIE Photonics West Conference, San Jose, CA.

[9] Pak, J., and Plumb, O. A., 1997, "Melting in a Two-Component Packed Bed," *Journal of Heat Transfer*, Vol. 119, pp. 553-559

[10] Zhang, Y., and Faghri, A., 1999, "Melting of a Subcooled Mixed Powder Bed with Constant Heat Flux Heating," *International Journal of Heat and Mass Transfer*, Vol. 42, pp. 775-788.

[11] Chen, T., and Zhang, Y., 2003, "Analysis of Melting in a Mixed Powder Bed with Finite Thickness Subjected to Constant Heat Flux Heating," *Proceeding of ASME Summer Heat Transfer Conference*, Las Vegas, NV.

[12] Zhang, Y., and Faghri, A., 1999, "Melting of a Subcooled Mixed powder Bed with Constant Heat Flux Heating," *International Journal of Heat and Mass Transfer*, Vol. 42, pp. 775-788.

[13] Kolossov, S., Boillat, E., Glardon, R., Fisher, P., and Locher, M., 2004, "3D FE Simulation for Temperature Evolution in the Selective Laser Sintering Process," *International Journal of Machine Tools and Manufacture*, vol. 44, 117-123.

[14] Zhang, Y., Faghri, A., Buckley, C. W., and Bergman, T. L., 2000, "Three-Dimensional Sintering of Two-Component Metal Powders with Stationary and Moving Laser Beams," *ASME J. Heat Transfer*, Vol. 122, pp. 150-158.

[15] Cao, Y. and Faghri, A., 1990, "A Numerical Analysis of Phase Change Problems Including Natural Convection," *Journal of Heat Transfer*, Vol. 112, pp. 812-816.

[16] Hardley, G. R., 1986, "Thermal Conductivity of packed Metal Powders," *International Journal of Heat and Mass Transfer*, Vol. 29, pp. 909-920.

[17] Kaviany, M., 1995, Principles of Heat Transfer in porous Media, Springer-Verlag, New York.

[18] Patankar, S. V., 1980, *Numerical Heat Transfer and Fluid Flow*, McGraw-Hill, New York.